BNL-108500-2015-JA

WILEY-VCH

DOI: 10.1002/((please add manuscript number))
Article type: Communication

Surface Profile Control of FeNiPt/Pt Core/Shell Nanowires for Oxygen Reduction Reaction

Huiyuan Zhu, Sen Zhang, Dong Su, Guangming Jiang and Shouheng Sun *

Dr. H. Zhu, Dr. S. Zhang, G. Jiang, Prof. S. Sun
Department of Chemistry
Brown University
Providence, RI 02912, USA
E-mail: ssun@brown.edu
Dr. D. Su
Center for Functional Nanomaterials
Brookhaven National Laboratory, Upton, NY 11973, USA

Keywords: Nanowires, multimetallic nanowires, core/shell, Pt-skin surface, oxygen reduction reaction

The ever-increasing energy demand requires renewable energy schemes with low environmental impacts. Electrochemical energy conversion devices, such as fuel cells, combine fuel oxidization and oxygen reduction reactions and have been studied extensively for renewable energy applications. However, their energy conversion efficiency is often limited by kinetically sluggish chemical conversion reactions, especially oxygen reduction reaction (ORR). [1-5] To date, extensive efforts have been put into developing efficient ORR catalysts with controls on catalyst sizes, compositions, shapes and structures.[6-12] Recently, Pt-based catalysts with core/shell and one-dimensional nanowire (NW) morphologies were found to be promising to further enhance ORR catalysis. With the core/shell structure, the ORR catalysis of a nanoparticle (NP) catalyst can be tuned by both electronic and geometric effects at the core/shell interface. [10,13,14] With the NW structure, the catalyst interaction with the conductive support can be enhanced to facilitate electron transfer between the support and the NW catalyst and to promote ORR. [11,15,16]

In this communication, we demonstrate that core/shell NW catalysis can be further optimized and the surface-smooth core/shell NWs are a new class of active and durable

catalyst for ORR. In recent studies of Pt catalysis for the ORR, early transition metals (M), such as Fe, Co, Ni, and Cu, are often alloyed with Pt to improve Pt catalysis and to lower the Pt usage. [9-14] However, these early transition metals are vulnerable to acid/electrochemical etching in the acidic electrochemical environment, leaving a Pt-skeleton type of structure with a large number of low coordination sites around Pt. [11,15] Such lowly coordinated Pt sites are subject not only to the strong binding to oxygenated species ("O") to "poison" the Pt surface during the ORR, but also to migration and dissolution, resulting in poor catalyst stability in the acidic ORR condition.[17-18] Studies on MPt thin film have indicated that reducing the roughness of Pt surface can improve Pt catalytic performance for ORR.[19,20] Recently, underpotential deposition and galvanic replacement of Cu into Pt has been reported to coat a monolayer of Pt onto Pd NWs. These Pd/Pt core/shell NWs were very active and durable for ORR due to the one-dimensional morphology and the smooth coating of Pt.[21,22] In our current study, we synthesize multimetallic core/shell FeNiPt/FePt NWs and then convert them into Pt-skeleton-type and Pt-skin-type FeNiPt/Pt NWs. Our electrocatalytic data show that the Pt-skin FeNiPt/Pt NWs are superior to the Pt-skeleton FeNiPt/Pt NWs in their catalysis for ORR, and the core/shell NWs are more efficient ORR catalysts than either FeNiPt NWs or the commercial Pt NPs.

The composition-controlled FeNiPt NWs were synthesized by varying the metal precursor ratios according to the previous report. [11] Here we chose $Fe_{36}Ni_{32}Pt_{32}$ (Fe: Ni: Pt~1) as the representative system to study the surface structure effect because this composition offered better ORR catalysis. [11] The FeNiPt/FePt core/shell NWs were made by the thermal decomposition of iron pentacarbonyl ($Fe(CO)_5$) and reduction of platinum acetylacetonate ($Pt(acac)_2$) in the presence of the $Fe_{36}Ni_{32}Pt_{32}$ NWs. The mass ratio between NW seeds and metal precursor was used to control the shell thickness. [16] For example, reacting 30 mg of FeNiPt NWs with 0.25 mmol $Pt(acac)_2$ and 0.25 mmol $Fe(CO)_5$ gave core/shell FeNiPt/FePt NWs with 1 nm FePt coating. **Figure S1** and **Figure 1A** show the typical transmission electron

microscopy (TEM) images of as-synthesized FeNiPt and FeNiPt/FePt core/shell NWs. The FeNiPt NWs have a dimension of 2.5 ± 0.2 nm (width) × 20-50 nm (length) (**Figure S1**). The length of the core/shell NWs is similar to the seeding NWs but their diameter is increased to 4.5 ± 0.3 nm, suggesting a 1 nm shell coating (**Figure 1A**). Previous reports have indicated that a 1 nm shell is necessary to form a uniform coating around core NPs and for the core/shell NPs to show the desired electronic and geometric effects on ORR. [23-24]

The as-synthesized FeNiPt/FePt NWs were first loaded on Ketjen carbon (C) (EC-300J) through sonicating the mixture of NW hexane dispersion and C till the solution became colorless (needed about 1 h). After washing with hexane and drying, the powder product, denoted as C-FeNiPt/FePt, was immersed in glacial acetic acid (AA) at 70 ^{o}C for 12 h. This AA treatment was used to remove the surfactant and surface Fe. [23] Inductively coupled plasma atomic emission spectroscopy (ICP-AES) was applied to track the transition metal ratio change during the process. The as-synthesized FeNiPt seeds have an atomic molar ratio of Fe: Ni: Pt=36:32:32. After FePt coating, the ratio is changed to Fe:Ni:Pt=42:12:46. After acid treatment, the final ratio is Fe: Ni: Pt=35:13:52. Since Ni:Pt is almost unchanged (from 12:46 to 13:52) and Fe:Pt decreases drastically (from 42:46 to 35:52), we can conclude that (1) the AA treatment etches only the surface Fe, and (2) the Ni and Fe in the core structure is effectively stabilized by the Pt shell.

We further annealed the etched core/shell sample in 95% argon + 5% hydrogen at 300 ^{o}C for 2 h to promote the “healing” of the defected surface, referred as Pt-skeleton, into skin-like surface.[25] This annealing condition was chosen to ensure that only Pt-skin surface was formed and NW morphology was still preserved, as shown in **Figure 1B**. Annealing at a higher temperature (such as 350 ^{o}C) could break the NWs (**Figure S2**). X-ray diffraction (XRD) patterns of the FeNiPt, FeNiPt/FePt, FeNiPt/Pt-skeleton and FeNiPt/Pt-skin NWs were collected and shown in **Figure S3**. They all show typical Pt-like face centred cubic (fcc) structure but their (111) peaks shift to higher angles than that of Pt, indicating the reduction of

fcc lattice in the NW alloy structures. The FeNiPt/FePt NWs have a narrower (111) peak than the FeNiPt NWs, inferring that the FePt coating and annealing lead to the increase in the fcc crystal domain size. Comparing the as-synthesized FeNiPt/FePt NWs with the etched ones, we can also see the (111) peak from the etched NWs shifts to lower angle (**Figure S3B**), indicating the enrichment of Pt in the NW structure after AA treatment.

The FeNiPt/Pt-skeleton and FeNiPt/Pt-skin structures were further characterized by high-angle annular dark field (HAADF)-scanning transmission electron microscopy (STEM), STEM-electron energy-loss spectroscopy (STEM-EELS) and high resolution TEM (HRTEM). **Figure 2A** and **Figure S4A** show typical HAADF-STEM images of a single FeNiPt/Pt-skin and FeNiPt/Pt-skeleton core/shell NW. Structural boundaries are clearly seen in these Z-contrast lattice images, demonstrating the formation of core/shell structure with the atom dislocation during the seed-mediated coating process. STEM-EELS of both core/shell NWs after AA treatment and thermal annealing (**Figure S4B** & **Figure 2B**) prove the formation of Pt-shell and FeNiPt-core structure. HRTEM image (**Figure 2C**) reveals a smoother surface around the FeNiPt/Pt-skin NW while humps are observed on the surface of the FeNiPt/Pt-skeleton NW.

The FeNiPt/Pt-skeleton and FeNiPt/Pt-skin core/shell NWs were further characterized electrochemically. To perform the electrochemical testing, the C-FeNiPt/Pt catalyst ink was prepared first (see experimental section) and 20 μL of this ink was deposited on the glassy carbon rotation disk electrode (GC-RDE) and dried at the ambient condition. **Figure 3A** shows the cyclic voltammetry (CV) scans of the commercial C-Pt (20% mass loading with Pt NP diameter of 2.5-3.5 nm, Fuel Cell Store), C-FeNiPt NWs (20% Pt-mass loading), C-FeNiPt/Pt-skeleton (21% Pt-mass loading) and C-FeNiPt/Pt-skin (25% Pt-mass loading) in 0.1 M $HClO_4$. In the potential range from 0.05 to 0.4 V, the characteristic hydrogen underpotential formation/stripping peaks of Pt surface were obtained and used to estimate the electrochemical active surface area (ECASA) of the catalyst according to previous report. [15]

The ECASA was also measured by electro-oxidation of adsorbed CO molecules (CO stripping). [15] **Figure 3B** and **Figure S5** show typical CO-stripping on FeNiPt/Pt-skeleton, FeNiPt/Pt-skin NWs and on commercial Pt surfaces. One major peak is observed between 0.71-0.72 V, followed by a shoulder peak at 0.78 V, which is more prominent on FeNiPt/Pt-skeleton than on FeNiPt/Pt-skin. This shoulder peak can be attributed to the oxidation of the adsorbed CO on the low coordination sites. [26] The suppressed shoulder peak on FeNiPt/Pt-skin surface indicates less low-coordination atoms presented on the surface, providing a clear evidence for the existence of a smoother surface structure. The ratio between ECASA values determined by hydrogen underpotential deposition ($ECASA_{Hupd}$) and by CO stripping ($ECASA_{CO}$) was summarized in **Table S1**. The $ECASA_{CO}$ was higher than $ECASA_{Hupd}$ in FeNiPt/Pt-skin structure, consistent with what has been observed on other Pt-skin surface. [27-28]

Electrocatalysis of these NWs on ORR was studied by linear scan voltammetry (LSV) from 0 to 0.8 V in 0.1 $HClO_4$ at a sweep rate of 10 mV/s and a GC-RDE rotation speed of 1600 rpm. The polarization curves related to ORR catalyzed by different kinds of NWs are summarized in **Figure 4A**. We can see that C-FeNiPt/Pt-skin NWs show a half-wave potential of 0.944 V, which is more positive than those of the C-Pt NPs (0.880 V), C-FeNiPt (0.904 V) and C-FeNiPt/Pt-skeleton NWs (0.932 V). The kinetic current was calculated from the LSV curve by mass-transport correction and further normalized to $ECASA_{Hupd}$ and Pt mass to generate both specific and mass activities for each catalyst. As a result, C-FeNiPt/Pt-skin NWs achieve the specific activity of 5.00 mA/cm^2 at 0.85 V and 2.02 mA/cm^2 at 0.90 V, respectively, higher than ultrathin FePt NWs reported previously[15] and FeNiPt NWs prepared in this report (1.25 mA/cm^2 at 0.85 V and 0.43 mA/cm^2 at 0.90 V). C-FeNiPt/Pt-skeleton NWs show the specific activity of 3.38 mA/cm^2 at 0.85 V and 1.22 mA/cm^2 at 0.90 V, while the commercial C-Pt NPs only show the specific activity of 1.41 mA/cm^2 (0.85V) and 0.28 mA/cm^2 (0.90V) (**Figure 4B**). The mass activities are also summarized in **Figure 4C**.

The C-FeNiPt/Pt-skin NWs have the largest value of 1160 mA/mg$_{Pt}$ at 0.85 V (473 mA/mg$_{Pt}$ at 0.90 V). Compared with all NWs studied (FeNiPt NWs have the mass activity of 440 mA/mg$_{Pt}$ at 0.85 V and 150 mA/mg$_{Pt}$ at 0.9 V; FeNiPt/Pt-skeleton NWs have the mass activity of 890 mA/mg$_{Pt}$ at 0.85 V and 324 mA/mg$_{Pt}$ at 0.9 V), the commercial C-Pt has the lowest value of 406 mA/mg$_{Pt}$ at 0.85 V (82 mA/mg$_{Pt}$ at 0.90 V). Clearly, the formation of the smoother Pt-surface around each FeNiPt/Pt-skin NW further increases the catalytic activity of the core/shell NW for the ORR.

Pt-based NWs are generally more stable than the NP counterparts in the ORR condition.[11, 15-16] The FeNiPt/Pt-skin core/shell NWs were also tested for the durability and were found to be the most stable catalyst among the Pt alloy NWs reported and the NWs described in this paper. **Figure 4D** and **Figure S6** summarizes the ORR polarization curves of different NWs before and after 10000 CV cycles in O_2-saturated 0.1 M $HClO_4$. The FeNiPt/Pt-skin NWs show almost no ECASA$_{Hupd}$ and activity drop (**Figure 4D**), while the FeNiPt/Pt-skeleton NWs have ~15% drop of their initial ECASA$_{Hupd}$ with the half-wave potential shifted negatively 9 mV (**Figure S6**). TEM images of FeNiPt/PT-skin NWs after the stability test proves that the morphology of these NWs are well preserved during the catalysis (**Figure S7**). These stability data further confirm that the coating of the Pt skin layer makes the Pt-catalyst more robust against Pt dissolution in the acidic ORR solution.[25]

In conclusion, we have synthesized FeNiPt/FePt core/shell NWs through a seed-mediated growth of FePt over the FeNiPt NWs. The surface profile of the core/shell NWs can be controlled through acid etching and thermal annealing to be either Pt-skeleton or Pt-skin structure with their 1-D morphology being maintained. These core/shell NWs show both higher activity and durability in catalyzing ORR in 0.1 M $HClO_4$ compared with the previously reported ultrathin NWs and the commercial Pt NPs. Owing to the fine tuning of the surface profile, the FeNiPt/Pt-skin NWs become the most efficient NW catalyst ever reported for ORR. The strategy demonstrated here can be extended to other NW catalyst systems,

providing a new approach to rational tuning of nanocatalysts for applications in energy conversion and other important chemical reactions.

Experimental Section

Synthesis of FeNiPt NWs: 0.2 sodium oleate (Na-oleate) was mixed with 12 mL 1-octadecene (ODE) and heated to 180 ^{o}C under a continuous N_2 flow and magnetic stirring to form a solution. After cooled down to room temperature, 0.5 mmol $Pt(acac)_2$ and 8 mL oleylamine (OAm) was added into the solution. The system was heated to 120 ^{o}C and 0.5 mmol $Fe(CO)_5$ was added into the solution under a N_2 blanket atmosphere. The solution was further heated to 160 ^{o}C and 0.5 mmol $Ni(acac)_2$ dissolved in the mixture of 2 mL OAm and 2 mL ODE was injected into the solution. The reaction solution was finally heated to 240 ^{o}C at a ramping rate of 3-4 ^{o}C/min and kept there for 1 h. After cooled down to 50 ^{o}C, the solution was transferred into two 50 mL centrifuge tubes and 25 mL isopropanol was added into each centrifuge tube to precipitate the NWs. The product was collected by centrifugation at 8500 rpm for 8 min. The obtained NWs were further washed by ethanol (25 mL) for three times and redispersed in hexane for further use.

Synthesis of FeNiPt/FePt NWs: 0.25 mmol $Pt(acac)_2$ was dissolved in 10 mL ODE in presence of 2 mL OAm and 1.5 mL oleic acid (OA). The solution was heated up to 115 ^{o}C for 30 min to remove the dissolved oxygen and moisture. Then 30 mg of the as-synthesized FeNiPt NWs in 2 mL hexane were added into the reaction solution as seeds. After 5 min, 0.25 mmol $Fe(CO)_5$ was added into the solution to initiate the nucleation on the existing seeds under a N_2 blanket atmosphere. The whole reaction solution was further raised to 220 ^{o}C at a rate of 3-4 ^{o}C and kept at this temperature for 30 min before it was cooled down to room temperature. The precipitation and purification process was same as in the FeNiPt NW synthesis.

Surface activation of FeNiPt/FePt NWs: 20 mg FeNiPt/FePt NWs was deposited on 20 mg carbon support through sonicating the mixture of NW hexane dispersion and Ketjen EC-300J Carbon (C) for 1 h. The C-FeNiPt/FePt NWs were precipitated out by centrifugation at 8500 rpm for 8min, and then mixed with 25 mL acetic acid (AA) and heated up to 70 ^{o}C under a gentle N_2 flow for 12 h to remove the surfactant and surface Fe. The C-FeNiPt/Pt NWs were washed first by deionized water and then by ethanol for two times to remove the excess AA and dried at ambient condition to form powder for further use.

Thermal annealing of the acid-treated sample at 300 ^{o}C for 2 h under a gentle forming gas flow was applied to produce C-FeNiPt/Pt-skin NWs.

Electrochemical Measurements: The commercial C-Pt, C-FeNiPt, C-FeNiPt/Pt-skeleton NWs or C-FeNiPt/Pt-skin NWs were suspended in a mixture of deionized water, isopropanol and Nafion (V/V/V=4/1/0.05) to form an ink. 20 μL ink (2 mg/mL) was deposited on the polished glassy carbon (GC) working electrode and dried at ambient condition. The catalysts were first cycled at 100 mV/s in 0.1 M $HClO_4$ until stable CVs were obtained. CVs at 50 mV/s in N_2-saturated $HClO_4$ were obtained to estimate $ECASA_{Hupd}$. CO stripping was obtained after CO bubbling at 0.1 V vs. RHE for 15 min. Linear scan voltammetry was conducted in an O_2-saturated 0.1 M $HClO_4$ solution by sweeping the potential from 0.26 to 1.06 V vs. RHE at 10 mV/s (1600 rpm). The stability test was studied by cycling potential between 0.66 V to 1.06 V at a rate of 100 mV/s for 10000 times in O_2-saturated 0.1 M $HClO_4$. Specific and mass activities were obtained at both 0.85 V and 0.9 V by dividing the kinetic current densities with the $ECASA_{Hupd}$ and Pt mass.

Supporting Information

Supporting Information is available from the Wiley Online Library or from the author.

Acknowledgements

This work was supported by the U.S. Army Research Laboratory and the U.S. Army Research Office under the Multi University Research Initiative (MURI, grant number W911NF-11-1-

0353) on "Stress-Controlled Catalysis via Engineered Nanostructures", and by the U.S. Department of Energy, Office of Energy Efficiency and Renewable Energy, Fuel Cell Technologies Program.

Received: ((will be filled in by the editorial staff))
Revised: ((will be filled in by the editorial staff))
Published online: ((will be filled in by the editorial staff))

[1] Y. Bing, H. Liu, L. Zhang, D. Ghosh, J. Zhang, *Chem. Soc. Rev*. **2010**, *39*, 2184.

[2] J. Chen, B. Lim, E. P. Lee, Y. Xia, *Nano Today* **2009**, *4*, 81.

[3] J. Suntivich, H. A. Gasteiger, N. Yabuuchi, H. Nakanishi, J. B. Goodenough, S. Yang, *Nat. Chem*. **2011**, *3*, 546.

[4] C. Cui, H. Li, J. Yu, M. Gao, S. Yu, *Angew. Chem. Int. Ed*. **2010**, *49*, 9149.

[5] H. Zhu, S. Zhang, Y. Huang, L. Wu, S. Sun, *Nano Lett*. **2013**, *13*, 2947.

[6] S. Guo, S. Zhang, S. Sun, *Angew. Chem. Int. Ed*. **2013**, *52*, 8526.

[7] C. Wang, H. Daimon, T. Onodera, T. Koda, S. Sun, *Angew. Chem. Int. Ed*. **2008**, *47*, 3588.

[8] J. Wu, L. Qi, H. You, A. Gross, J. Li, H. Yang, *J. Am. Chem. Soc.* **2012**, *134*, 11880.

[9] C. Wang, D. van der Vliet, K. Chang, H. You, D. Strmcnik, J. A. Schlueter, N. M. Markovic, V. R. Stamenkovic, *J. Phys. Chem. C* **2009**, *113*, 19365.

[10] S. Zhang, X. Zhang, G. Jiang, H. Zhu, S. Guo, D. Su, G. Lu, S. Sun, *J. Am. Chem. Soc.*, **2014**, *136*, 7734.

[11] H. Zhu, S. Zhang, S. Guo, D. Su, S. Sun, *J. Am. Chem. Soc.*, **2013**, *135*, 7130.

[12] C. Cui, L. Gan, M. Heggen, S. Rudi, P. Strasser, *Nat. Mater*. **2013**, *12*, 765.

[13] C. Wang, D. Li, M. Chi, J. Pearson, R. B. Rankin, J. Greeley, Z. Duan, G. Wang, D. van der Vliet, K. L. More, N. M. Markovic, V. R. Stamenkovic, *J. Phys. Chem. Lett*. **2012**, *3*, 1668.

[14] C. Cui, L. Gan, H. Li, S. Yu, M. Heggen, P. Strasser, *Nano Lett*. **2012**, *12*, 5885.

[15] S. Guo, D. Li, H. Zhu, S. Zhang, N. M. Markovic, V. R. Stamenkovic, S. Sun, *Angew. Chem. Int. Ed.* **2013**, *52*, 3465.

[16] S. Guo, S. Zhang, D. Su, S. Sun, *J. Am. Chem. Soc*., **2013**, *135*, 13879.

[17] K. J. J. Mayrhofer, B. B Blizanac, M. Arenz, V. R. Stamenkovic, N. M. Markovic, *J. Phys. Chem. B* **2005**, *109*, 14433.

[18] R. Borup, J. Meyers, B. Pivovar, Y. S. Kim, R. Mukundan, N. Garland, D. Myers, M. Wilson, F. Garzon, D. Wood, P. Zelenay, K. More, K. Stroh, T. Zawodzinski, J. Boncella, J. E. McGrath, M. Inaba, K. Miyatake, M. Hori, K. Ota, Z. Ogumi, S. Miyata, A. Nishikata, Z. Siroma, Y. Uchimoto, K. Yasuda, K. Kimijima, N. Iwashita, *Chem. Rev.* **2007**, *107*, 3904.

[19] V. R. Stamenkovic, B. Fowler, B. S. Mun, G. Wang, P. N. Ross, C. A. Lucas, N. M. Markovic, *Science* **2007**, *315*, 493.

[20] V. R. Stamenkovic, B. S. Mun, M. Arenz, K. J. J. Mayrhofer, C. A. Lucas, G. Wang, P. N. Ross, N. M. Markovic, *Nat. Mater*. **2007**, *6*, 241.

[21] K. Gong, J. Park, D. Su, R. R. Adzic, J. Solid State Electrochem. 2014, 18, 1171.

[22] C. Koenigsmann, A. C. Santulli, K. Gong, M. B. Vukmirovic, W. Zhou, E. Sutter, S. S. Wong, R. R. Adzic, J. Am. Chem. Soc. 2011, 133, 9783.

[23] V. Mazumder, M. Chi, K. L. More, S. Sun, *J. Am. Chem. Soc*. **2010**, *132*, 7848.

[24] S. Zhang, Y. Hao, D. Su, V. V. T. Doan-Nguyen, Y. Wu, J. Li, S. Sun, C. B. Murray, *J. Am. Chem. Soc.* **2014**, *136*, 15921.

[25] C. Wang, M. Chi, D. Li, D. Strmcnik, D. van der Vliet, G. Wang, V. Komanicky, K. Chang, A. P. Paulikas, D. Tripkovic, J. Pearson, K. L. More, N. M. Markovic, V.R. Stamenkovic, *J. Am. Chem. Soc*. **2011**, *133*, 14396.

[26] S. Brimaud, Z. Jusys, R. J. Behm, *Beilstein J. Nanotechnol.* **2014**, *5*, 735.

[27] C. Chen, Y. Kang, Z. Huo, Z. Zhu, W. Huang, H. Xin, J. D. Snyder, D. Li, J. A. Herron, M. Mavrikakis, M. Chi, K. L. More, Y. Li, N. M. Markovic, G. A. Somorjai, P. Yang, V. R. Stamenkovic, *Science* **2014**, *343*, 1339.

[28] D. F. van der Vliet, C. Wang, D. Li, A. P. Paulikas, J. Greeley, R. B. Rankin, D. Strmcnik, D. Tripkovic, N. M. Markovic, V. R. Stamenkovic, *Angew. Chem. Int. Ed.* **2012**, *51*, 3139.

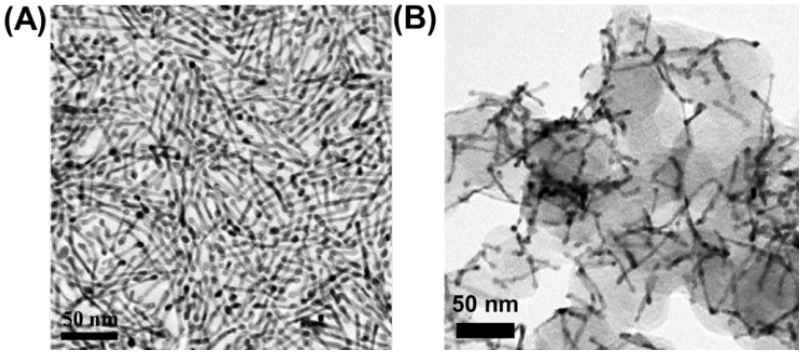

Figure 1. TEM images of the as-synthesized FeNiPt/FePt core/shell NWs (A) and C-FeNiPt/FePt after acetic acid treatment and thermal annealing (B).

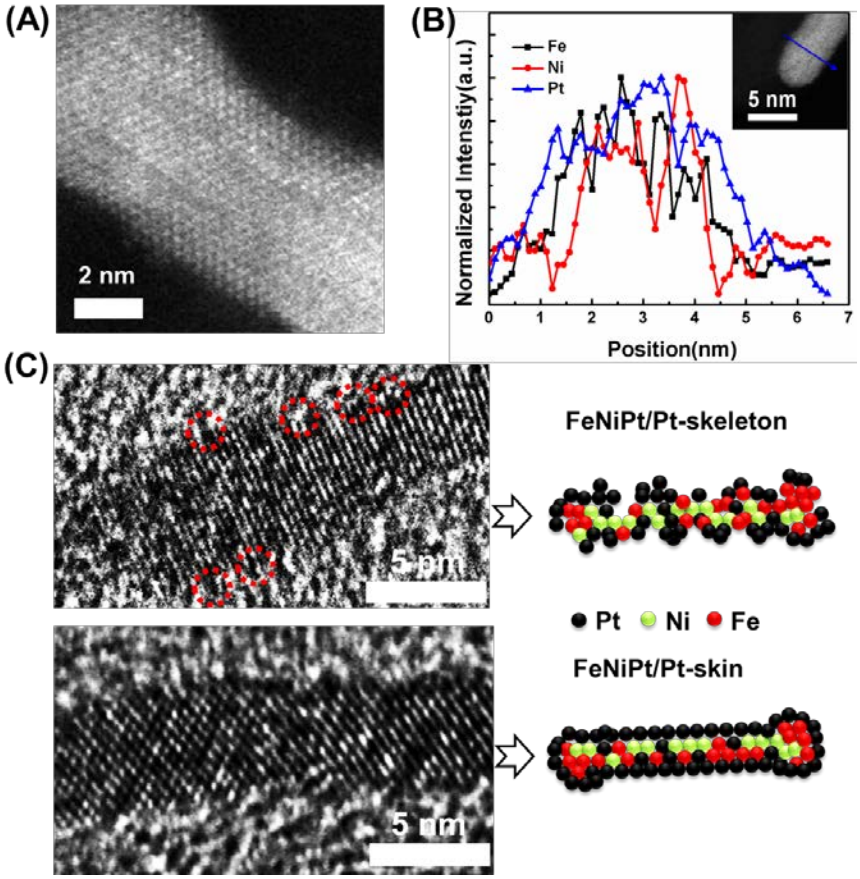

Figure 2. (A) HAADF-STEM image and (B) STEM-EELS line scan of the FeNiPt/Pt-skin NWS. (C) HRTEM images and schematic illustration of FeNiPt/Pt-skeleton and FeNiPt/Pt-skin NWs.

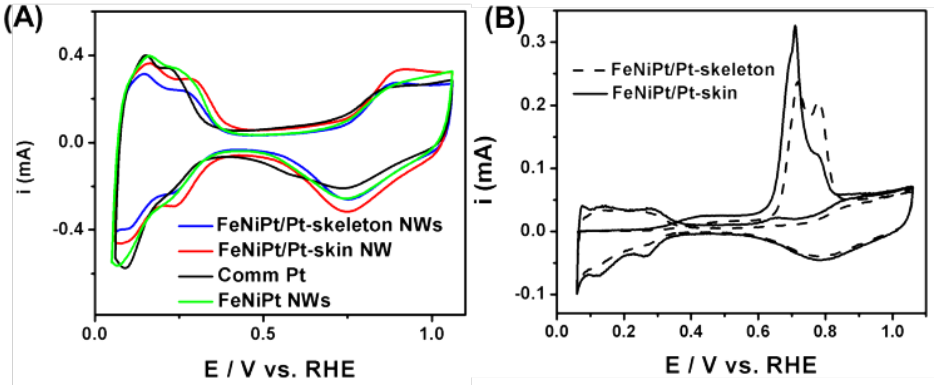

Figure 3. (A) CVs of the commercial C-Pt NPs, C-FeNiPt, C-FeNiPt/Pt-skeleton and C-FeNiPt/Pt-skin NWs. (B) CO-stripping curves for the FeNiPt/Pt-skeleton and FeNiPt/Pt-skin NWs.

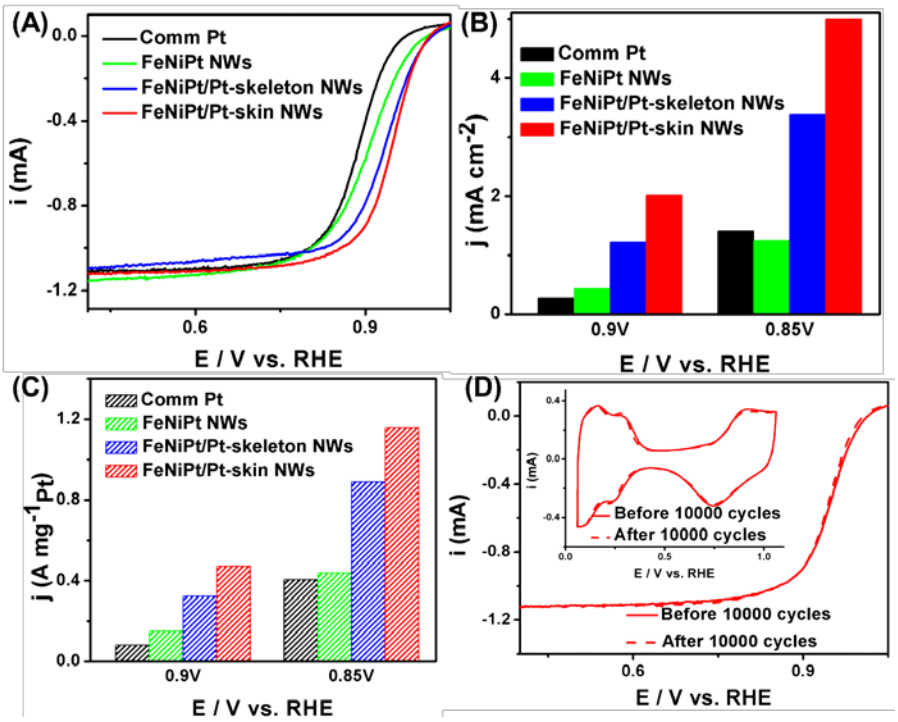

Figure 4. (A) Polarization curves obtained from the catalyst-rotating disk electrode (1600 rpm), (B) specific activities and (C) mass activities of the commercial C-Pt NPs, C-FeNiPt, C-FeNiPt/Pt-skeleton and C-FeNiPt/Pt-skin NWs. (D) Polarization curves of the C-FeNiPt/Pt-skin NWs before and after 10000 potential cycles (inset: CVs of the NWs before and after 10000 potential cycles).

Monodisperse core/shell FeNiPt/FePt Nanowires (NWs) (4.5 x 20-50 nm) are synthesized by seed-mediated growth of FePt over the pre-made 2.5 nm wide FeNiPt NWs. The surface profile of the as-synthesized FeNiPt/FePt NWs is further tailored by acid and thermal treatment and the core/shell NWs are converted to either FeNiPt/Pt-skeleton or FeNiPt/Pt-skin NWs. The FeNiPt/Pt-skin NWs show higher activities (5.00 mA/cm^2 and 1160 mA/mg$_{Pt}$ at 0.85 V vs. RHE) than the FeNiPt/Pt-skeleton NWs. The work demonstrates a rational approach to the further catalytic enhancement of core/shell NWs for the oxygen reduction reaction.

Keyword

Nanowires, multimetallic nanowires, core/shell, Pt-skin surface, oxygen reduction reaction

Huiyuan Zhu, Sen Zhang, Dong Su, Guangming Jiang and Shouheng Sun *

Surface Profile Control of FeNiPt/Pt Core/Shell Nanowires for Oxygen Reduction Reaction

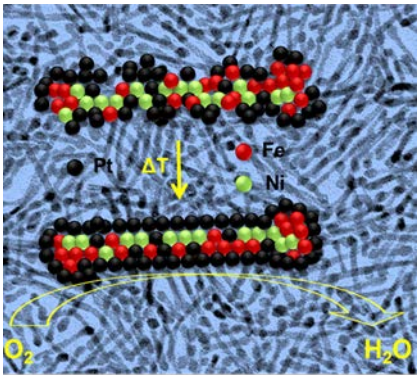

Copyright WILEY-VCH Verlag GmbH & Co. KGaA, 69469 Weinheim, Germany, 2013.

Supporting Information

Surface Profile Control of FeNiPt/Pt Core/Shell Nanowires for Oxygen Reduction Reaction

*Huiyuan Zhu, Sen Zhang, Dong Su, Guangming Jiang and Shouheng Sun**

Experimental Section

Materials. Oleylamine (OAm, >70%), oleic acid (OA), sodium oleate (Na-oleate) 1-octadecene (ODE), $Pt(acac)_2$ (acac = aceylacetonate), $Ni(acac)_2$, $Fe(CO)_5$, hexane, isopropanol, ethanol and Nafion (5%) were all purchased from Sigma Aldrich.

Characterization. TEM images were obtained from a Philips CM 20 operating at 200 kV. The inductively coupled plasma-atomic emission spectroscopy (ICP-AES) measurements were carried on a JY2000 Ultrace ICP atomic emission spectrometer equipped with a JY AS 421 autosampler and 2400g/mm holographic grating. X-ray diffraction (XRD) characterization was carried out on a Bruker AXS D8-Advanced diffractometer with Cu Kα radiation (λ =1.5418 Å). HRTEM images were acquired on JEOL 2100F (200 kV). STEM analyses were performed on a Hitachi HD2700C (200 kV) with a probe aberration-correction in the Center for Functional Nanomaterial at Brookhaven National Laboratory. Electrochemical measurements were carried out on an Autolab potentiostat from Metrohm Instrument Company (Autolab 302). A three-electrode system consisting of a glassy carbon (GC) working electrode (5-mm in diameter), an Ag/AgCl reference electrode (in 4 M KCl) and a platinum wire counter electrode was used for electrochemical study. All the potentials were calibrated versus reversible hydrogen electrode (RHE).

Figures

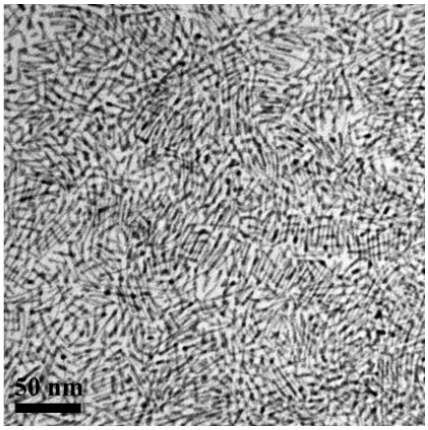

Figure S1. TEM image of the as-synthesized FeNiPt NWs.

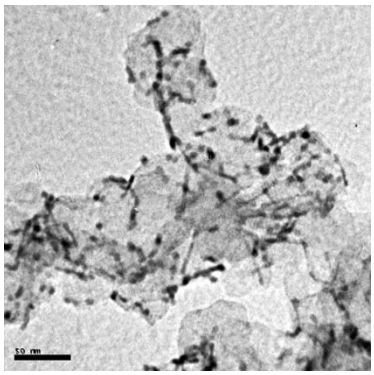

Figure S2. TEM images of the C-FeNiPt/FePt NWs after acid treatment and thermal annealing at 350 ^{o}C for 2 h.

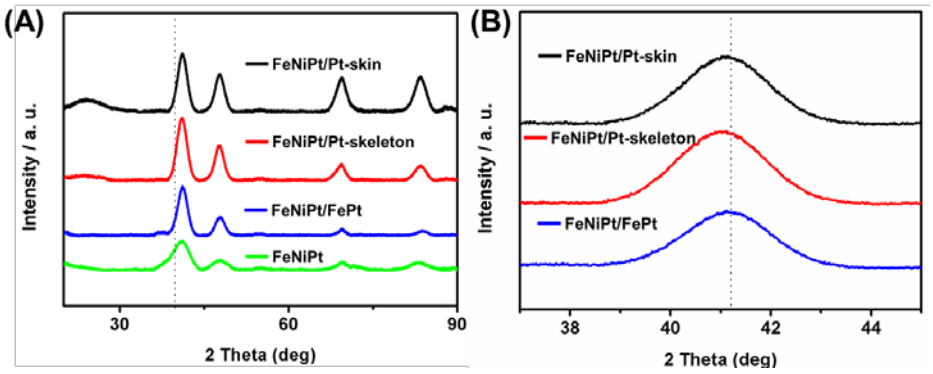

Figure S3. (A) XRD patterns of FeNiPt, FeNiPt/FePt, FeNiPt/Pt-skeleton and FeNiPt/Pt-skin NWs (dashed line indicates the position of the standard (111) peak of the bulk Pt). (B) (111) peak positions of FeNiPt/FePt, FeNiPt/Pt-skeleton and FeNiPt/Pt-skin NWs.

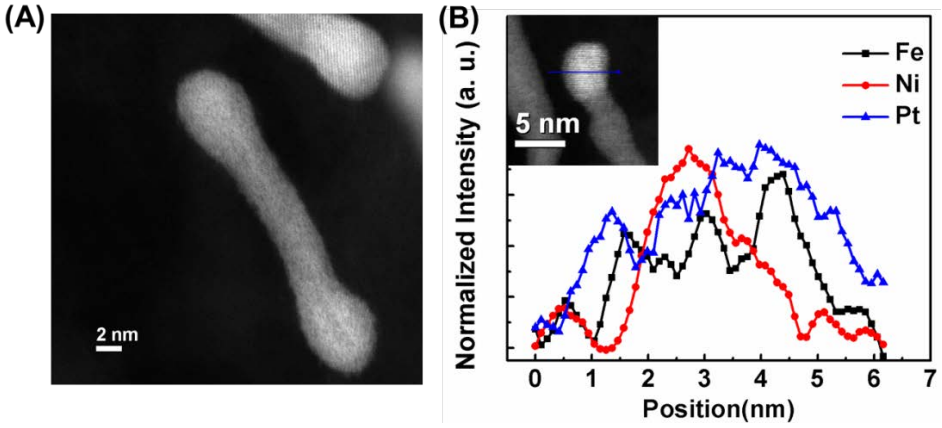

Figure S4. (A) HAADF-STEM image and (B) STEM-EELS line scan of a single FeNiPt/Pt-skeleton NW.

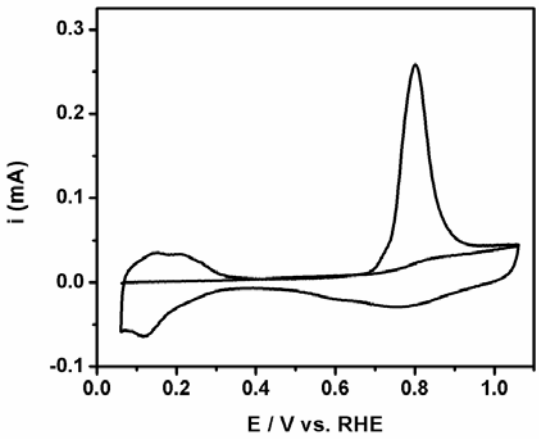

Figure S5. CO-stripping curves for the commercial C-Pt NPs.

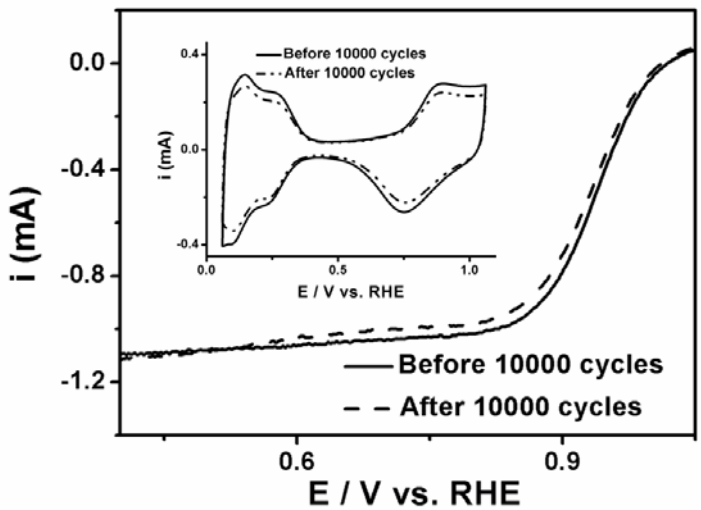

Figure S6. Polarization curves of the C-FeNiPt/Pt-skeleton NWs before and after 10000 potential cycles (inset: CVs of the C-FeNiPt/Pt-skeleton NWs before and after 10000 potential cycles).

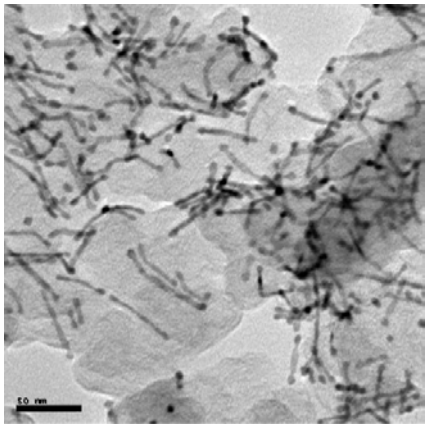

Figure S7. TEM image of C-FeNiPt/Pt-skin NWs after stability test.

Table S1

	FeNiPt/Pt-skeleton	FeNiPt/Pt-skin	Commercial Pt
$ECASA_{co}/ECASA_{Hupd}$	1.03	1.12	1.00